



HAL
open science

THE EFFECTS OF KINETIC INSTABILITIES ON SMALL-SCALE TURBULENCE IN EARTH'S MAGNETOSHEATH

H. Breuillard, E. Yordanova, A. Vaivads, O. Alexandrova

► **To cite this version:**

H. Breuillard, E. Yordanova, A. Vaivads, O. Alexandrova. THE EFFECTS OF KINETIC INSTABILITIES ON SMALL-SCALE TURBULENCE IN EARTH'S MAGNETOSHEATH. *The Astrophysical Journal*, 2016, 829 (1), pp.54. 10.3847/0004-637X/829/1/54 . hal-02457992

HAL Id: hal-02457992

<https://hal.science/hal-02457992v1>

Submitted on 11 Mar 2020

HAL is a multi-disciplinary open access archive for the deposit and dissemination of scientific research documents, whether they are published or not. The documents may come from teaching and research institutions in France or abroad, or from public or private research centers.

L'archive ouverte pluridisciplinaire **HAL**, est destinée au dépôt et à la diffusion de documents scientifiques de niveau recherche, publiés ou non, émanant des établissements d'enseignement et de recherche français ou étrangers, des laboratoires publics ou privés.



THE EFFECTS OF KINETIC INSTABILITIES ON SMALL-SCALE TURBULENCE IN EARTH'S MAGNETOSHEATH

H. BREUILLARD¹, E. YORDANOVA¹, A. VAIVADS¹, AND O. ALEXandrova²

¹Swedish Institute of Space Physics, IRF Uppsala, Sweden; hbreuill@gmail.com

²LESIA/Observatoire de Paris-Meudon, Meudon, France

Received 2016 January 13; revised 2016 June 27; accepted 2016 June 28; published 2016 September 21

ABSTRACT

The Earth's magnetosheath is the region delimited by the bow shock and the magnetopause. It is characterized by highly turbulent fluctuations covering all scales from MHD down to kinetic scales. Turbulence is thought to play a fundamental role in key processes such as energy transport and dissipation in plasma. In addition to turbulence, different plasma instabilities are generated in the magnetosheath because of the large anisotropies in plasma temperature introduced by its boundaries. In this study we use high-quality magnetic field measurements from *Cluster* spacecraft to investigate the effects of such instabilities on the small-scale turbulence (from ion down to electron scales). We show that the steepening of the power spectrum of magnetic field fluctuations in the magnetosheath occurs at the largest characteristic ion scale. However, the spectrum can be modified by the presence of waves/structures at ion scales, shifting the onset of the small-scale turbulent cascade toward the smallest ion scale. This cascade is therefore highly dependent on the presence of kinetic instabilities, waves, and local plasma parameters. Here we show that in the absence of strong waves the small-scale turbulence is quasi-isotropic and has a spectral index $\alpha \approx -2.8$. When transverse or compressive waves are present, we observe an anisotropy in the magnetic field components and a decrease in the absolute value of α . Slab/2D turbulence also develops in the presence of transverse/compressive waves, resulting in gyrotropy/non-gyrotropy of small-scale fluctuations. The presence of both types of waves reduces the anisotropy in the amplitude of fluctuations in the small-scale range.

Key words: Earth – instabilities – turbulence – waves

1. INTRODUCTION

Space plasmas are commonly in a turbulent state that is characterized by large and irregular fluctuations of the physical parameters (e.g., density, velocity, and electromagnetic field) from the largest (MHD) down to the smallest (electron) scales. Turbulence is a natural way to convert the energy of large-scale motions into small-scale fluctuations. The energy cascades by nonlinear interactions among eddies from MHD to kinetic (proton and electron) scales, where it is eventually dissipated into plasma heating (see the review by Bruno & Carbone 2013). It is believed that at kinetic scales turbulence plays a fundamental role in energy dissipation and plasma heating (Schekochihin et al. 2009). Therefore, it is crucial to characterize the properties of kinetic turbulence (e.g., scaling law, anisotropy), the governing processes (e.g., wave-particle interactions), and the resulting coherent structures (see Alexandrova et al. 2013).

Examples of turbulent space plasmas are stellar winds, the solar wind, and planetary magnetosheaths. Earth's magnetosheath—the interface region between the solar wind and the terrestrial magnetosphere—is a region of particular interest in which to study turbulence (Zimbaro et al. 2010). The magnetosheath forms as the plasma of the solar wind is decelerated and heated at the bow shock and flows around the Earth's magnetosphere. The proximity of the terrestrial magnetosheath makes it the best laboratory in which to investigate in situ the features of turbulence in collisionless plasma and to understand the solar-terrestrial interactions, i.e., the transport of mass and energy from the solar wind to the magnetosphere. The pile-up of the magnetosheath plasma in front of the Earth's magnetosphere introduces an important ion temperature anisotropy $T_{\perp i} > T_{\parallel i}$ (parallel and perpendicular to

the magnetic field), causing various kinetic instabilities (Schwartz et al. 1996) that affect the plasma turbulence (see, e.g., Bale et al. 2009).

The presence of various fluid and kinetic instabilities implies that linearly unstable waves can grow and propagate in this region (see, e.g., Zimbaro et al. 2010). A rich variety of low-frequency (below the ion gyrofrequency f_{ci}) waves is observed in Earth's magnetosheath (see the review by Schwartz et al. 1996). According to observations and kinetic linear theory, two wave modes seem to dominate the magnetosheath due to the ion anisotropy $T_{\perp i} > T_{\parallel i}$, which pervades throughout. The Alfvén/ion-cyclotron (AIC) mode grows readily under conditions where the ion plasma beta β_i is typically below 1. AIC is a left-hand circularly polarized wave for parallel propagation in the plasma rest frame ($\mathbf{k} \parallel \mathbf{B}_0$, where \mathbf{k} is the wave vector and \mathbf{B}_0 is the background magnetic field). AIC is cyclotron-resonant with the ions and its growth rate is positive in the frequency range $f \sim 0.1 - 0.7f_{ci}$ with a maximum at $\sim 0.5f_{ci}$ (Schwartz et al. 1996). At higher β_i (typically above 3), mirror modes (zero-frequency waves in the plasma rest frame) usually dominate the power spectra at low frequencies. A mirror mode is a compressive ($\delta B_{\parallel} \gg \delta B_{\perp}$) slow mode with $\mathbf{k} \perp \mathbf{B}_0$ and it is linearly polarized with antiphase variations in the density and the magnitude of the magnetic field (Shevyrev et al. 2006). Under conditions of intermediate β_i ($1 \leq \beta_i \leq 3$), both AIC and mirror-wave modes are usually observed (see, e.g., Alexandrova et al. 2013).

It has long been known that at frequencies corresponding to the ion scales Doppler-shifted by the plasma flow velocity, the power spectrum of turbulent fluctuations steepens. In the solar wind the steepening is typically seen at frequencies $f_{sc} \sim 0.1$

–1 Hz (Russell 1972; Alexandrova et al. 2013; Bruno & Carbone 2013). It is attributed to a change in the nature of turbulence at these scales. It has been shown that in the solar wind (see Hellinger et al. 2006; Matteini et al. 2007, 2013; Bale et al. 2009), plasma instabilities can have an important impact on the power spectral density (PSD) of the magnetic field, because the fluctuations and compressibility are enhanced along the thresholds of the temperature anisotropy. Therefore, it is important to understand the role of these local instabilities in order to be able to interpret correctly the physical processes of dissipation at the kinetic scales.

In a case study (Sahraoui et al. 2006) where the *Cluster* spacecraft was located in the magnetosheath close to the magnetopause, the effects of the latter and mirror modes on the k -vector small-scale turbulence were investigated. The authors stated that the magnetopause was acting as an external constraint, preventing the cascade from developing in the direction normal to it, and that this, as well as the presence of mirror-mode structures, could affect the spectral index and the anisotropy of k fluctuations in the small-scale range. The results of Sahraoui et al. (2006) also emphasized the importance of the Doppler shift in the measured temporal spectra.

The spectral index and anisotropy of the amplitude of magnetic fluctuations in the magnetosheath have been investigated in Alexandrova et al. (2008b): In the small-scale frequency range, δB_{\perp}^2 and δB_{\parallel}^2 are generally observed to follow a similar power law f^{α} with $-3 \leq \alpha \leq -2$, and usually $\delta B_{\perp}^2 > \delta B_{\parallel}^2$, except for the largest $\beta_i (> 5)$ where $\delta B_{\perp}^2 \sim \delta B_{\parallel}^2$. In particular, when large mirror modes seem to be observed (i.e., a strong parallel component below f_{ρ_i}), the spectral index of the parallel component in the small-scale range is decreased, modifying the global index (see Figure 7 in Alexandrova et al. 2008b). At small scales, the turbulence is also observed to be non-gyrotropic: the energy along the direction perpendicular to ν and \mathbf{B} is larger than the energy along the projection of ν in the plane perpendicular to \mathbf{B} . This non-gyrotropy has been attributed to the presence of 2D turbulence (i.e., $k_{\perp} \gg k_{\parallel}$), whereas in the case of slab turbulence (i.e., $k_{\parallel} \gg k_{\perp}$) the fluctuations are gyrotropic (see Bieber et al. 1996; Matthaeus et al. 2007). Alexandrova et al. (2008b) argued that this non-gyrotropy might be reinforced by different Doppler shifts for fluctuations with k parallel and perpendicular to ν in the plane perpendicular to \mathbf{B} .

In addition to the spectral index α , indicating how the energy is transferred between scales, it is important to identify the scale associated with the spectral break (e.g., Alexandrova et al. 2013). Several ion kinetic scales have been associated with the break, most notably the ion gyroradius ρ_i and ion inertial length λ_i (for details, see Chen et al. 2014, and references therein). These scales are related to different physical processes, respectively kinetic Alfvén turbulence (Schekochihin et al. 2009) for ρ_i and Hall–MHD (Galtier 2006) or the thickness of current sheets (Leamon et al. 2000; Dmitruk et al. 2004) for λ_i . In a solar wind with $\beta \approx 1$ different effects can be at work at ion scales, and it is difficult to associate one scale with a break (see, e.g., Lion et al. 2016). To address this question, in a recent study Chen et al. (2014) investigated exceptional intervals in the solar wind with $\beta_i \ll 1$ and $\beta_i \gg 1$ and concluded that the ion spectral break occurs at the larger of the two scales.

Czaykowska et al. (2001) showed that, similarly to the solar wind, in the magnetosheath there is a break in the spectrum, with the spectral index going from about $\alpha \sim -1$ below the proton gyrofrequency to $\alpha \sim -2.6$ above it. In this study, the authors also observed a “knee” (i.e., a local and broad maximum) at the spectral break, which was interpreted as the signature of AIC waves. Nonlinear structures such as Alfvén vortices have also been associated with the knee (Alexandrova et al. 2006, 2008b). In Alexandrova et al. (2006), Alfvén vortices were observed to be controlled by λ_i , i.e., by the largest scale (for this particular case $\beta_i < 1$), in agreement with Chen et al. (2014). However, to the authors’ knowledge, the scale at which the ion spectral break occurs for conditions of higher β_i in the magnetosheath has not been reported yet.

In this work we analyze *Cluster* spacecraft measurements in Earth’s magnetosheath to investigate at what scale the power spectrum of magnetic field fluctuations breaks and what the effect is of kinetic instabilities on small-scale plasma turbulence. First, we select events with different plasma parameters (β_i and the bulk velocity vector ν) to clearly separate spatial and temporal scales, and determine at which one the break eventually occurs (Section 2). Then, we focus on time intervals with different dominant kinetic waves (i.e., mirror modes and AIC waves) and investigate their respective effects on the spectral index and anisotropy of fluctuations in the small-scale range of the spectrum (Section 3). Finally, we conclude the paper with a discussion and summary of the results (Section 4).

2. ION-SCALE SPECTRAL BREAK

In this section we first present the data processing we used to obtain the PSDs shown in the different figures. We use waveform data measured by the FGM (Balogh et al. 2001) and STAFF (Cornilleau-Wehrin et al. 1997) instruments on board *Cluster* spacecraft, which are merged, allowing us to study fluctuations with frequencies up to 12.5 Hz, which covers the ion scales. To combine the data from the two instruments, we apply a finite impulse filter, where FGM has been low-passed and STAFF has been high-passed with the same cutoff frequency of ~ 1 Hz. We use a low-pass filter at 0.01 Hz to define the background magnetic field \mathbf{B}_0 and $\delta \mathbf{B} = \mathbf{B} - \mathbf{B}_0$. This value has been chosen because in our cases it is the closest to the ion scales but does not affect the spectra (notably mirror modes that have a typical frequency of 0.025–0.05 Hz in the three cases shown). The ratio $\delta B/B_0$ is on average ~ 0.125 using this low-pass filter value for all cases analyzed in this paper, thus the mean-field approximation is appropriate here. Then we define a reference frame based on \mathbf{B}_0 and ν , as follows: the z component is chosen parallel to \mathbf{B}_0 , x is perpendicular to \mathbf{B}_0 in the plane containing \mathbf{B}_0 and ν , and y completes the direct orthonormal frame (see, e.g., Bieber et al. 1996; Alexandrova et al. 2006). This reference frame is reconstructed every 4 s, which is the velocity sampling rate provided by CIS (Rème et al. 2001). Wavelet analysis (Morlet mother wavelet, see Torrence & Compo 1998) is then employed to compute the PSD of each δB component and the total δB . To help better identify waves and structures, we also make use of the WHAMP program (Rönmark 1982) to calculate the growth rate and we compute the polarization of δB waveforms as well (not shown).

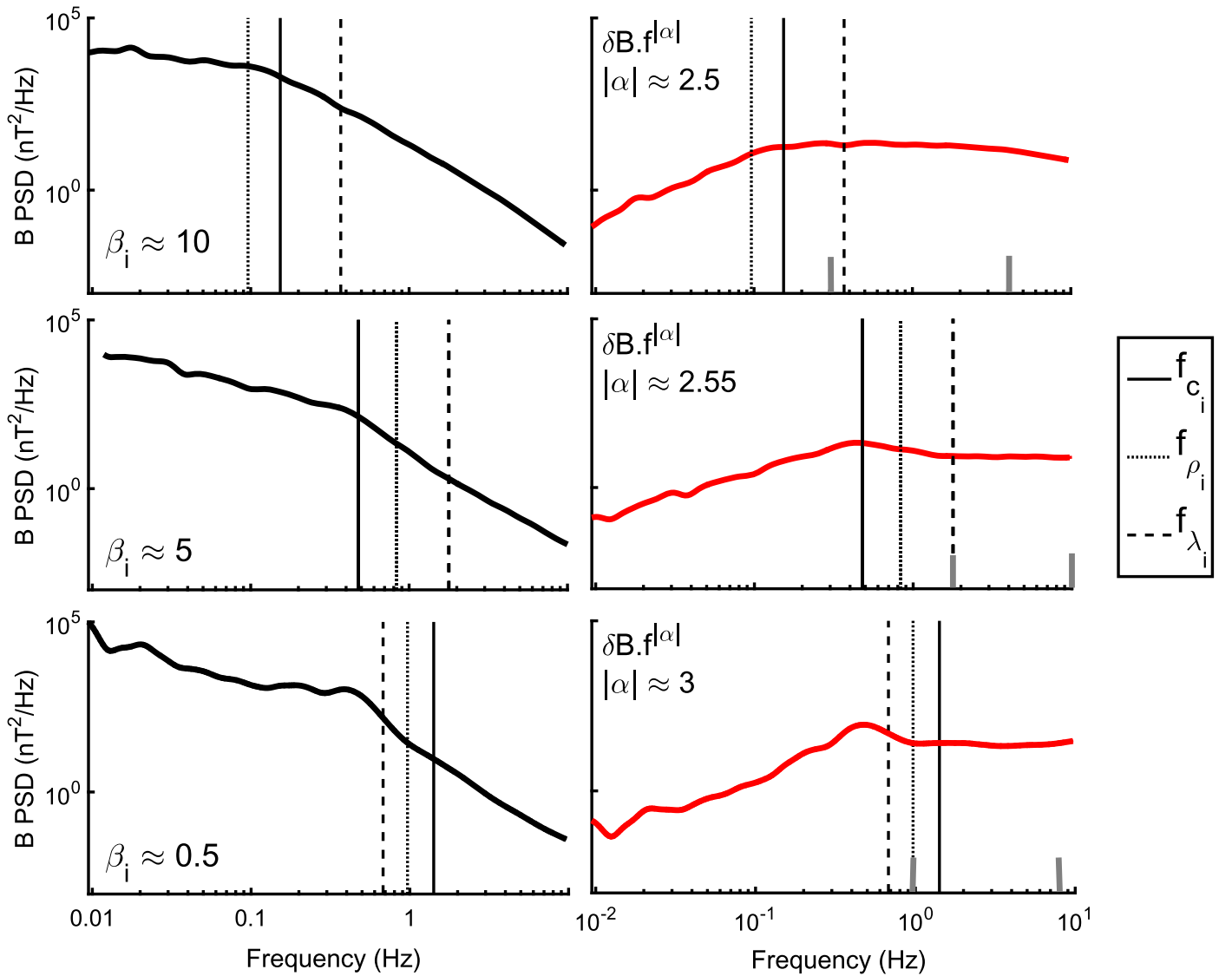


Figure 1. PSDs of δB measurements on board *C3* on 2001 March 16 at 13:00–13:20 UT (top panel), 2001 December 16 at 06:10–06:30 (middle panel), and 2001 March 31 at 16:57–17:12 (bottom panel). Black thick solid lines indicate the total δB PSD and red thick solid lines indicate the compensated PSD $\delta B \times f^{|\alpha|}$. The plasma β_i of each case is indicated on each panel, along with the absolute value of the spectral index $|\alpha|$, computed between the two gray vertical lines. The ion gyrofrequency (solid), Doppler-shifted gyroradius scale (dotted), and Doppler-shifted inertial length (dashed) are denoted by black vertical lines.

Figure 1 shows the PSDs of the magnetic field for the three selected time intervals of 15–20 minutes each. The data have been recorded on *Cluster 3* (*C3*) under different plasma conditions in the magnetosheath. Each case shows a different ion scale ($f_{c_i}, f_{\rho_i}, f_{\lambda_i}$) as the largest: (1) high beta $\beta_i \sim 10$ (with f_{ρ_i} as the largest scale) from 2001 March 16, 13:00–13:20 UTC (top panel); (2) another case of high beta $\beta_i \sim 5$ (but with f_{c_i} as the largest scale) from 2001 December 16, 06:10–06:30 UTC (intermediate panel); and (3) low beta $\beta_i \sim 0.5$ (with f_{λ_i} as the largest scale) from 2001 March 31, 16:57–17:12 UTC (bottom panel). In all cases $v \approx 200 \text{ km s}^{-1}$; however, high/low β_i allows us to clearly separate f_{ρ_i} from f_{λ_i} (shown in Figure 1 by dotted and dashed vertical lines in each panel, respectively). The transformation from spatial to time domain is done assuming Taylor’s hypothesis.

In all cases of Figure 1 a spectral break is observed at the largest of the three scales, i.e., the scale corresponding to the lowest ion frequency f_{\min_i} . This result is consistent with the observations in the solar wind (Chen et al. 2014). However, in

the range $f_{\min_i} \leq f \leq f_{\max_i}$, where f_{\max_i} is the frequency corresponding to the smallest ion scale, the power spectra are modified by ion instabilities: while a power law seems to develop after the break in the case of very high beta (Figure 1, top panel), the onset of the cascade is shifted toward higher frequencies (Figure 1, middle and bottom panels) by the formation of a broader “knee” and develops at $f > f_{\max_i}$. For example, in the bottom panel, we observe a local bump at the break, which has been identified in this particular event (see Alexandrova et al. 2006) as the signature of Alfvén vortices, controlled by f_{λ_i} . Each case presents a different slope α in this range, as shown by the compensated spectra $\delta B^2 \times f^{-\alpha}$ depicted by red lines in each panel (the spectral index α is indicated in each panel on the right).

Kinetic instabilities can modify the power spectrum at ion scales and affect the fluctuations in the small-scale range. Therefore, the identification of kinetic instabilities is important and it is the subject of investigation in the following section.

3. SMALL-SCALE TURBULENCE ANISOTROPY AND SPECTRAL INDEX

In this section we study in detail the effects of mirror modes and AIC waves, which are observed to dominate in the magnetosheath (Schwartz et al. 1996), on the spectral index and anisotropy of fluctuations in the small-scale range, i.e., $f \in [0.2\text{--}10]$ Hz in our case. To do so, we choose four time intervals of about 3–5 minutes each (i.e., PSDs at frequencies < 0.025 Hz are not reliable) and we sort them out depending on the nature of the present waves. The selected cases are chosen as follows: (1) no waves are dominating the spectrum (2008 March 17, 12:30–12:35 UTC); (2) only strong mirror modes are observed (2008 March 25, 07:01–07:05 UTC); (3) strong AIC waves dominate (2008 March 30, 01:35–01:39 UTC); and (4) a mixture of the mirror and AIC waves is observed (2008 March 25, 06:51–06:56 UTC). These intervals are selected during periods of low v ($v \approx 50 \text{ km s}^{-1}$) so that the effects of the Doppler shift due to the plasma flow past the spacecraft (i.e., increase of δB_y) are minimized (Sahraoui et al. 2006; Alexandrova et al. 2008b). Because of the low bulk velocity Taylor’s hypothesis could be violated (see, e.g., Klein et al. 2014), thus we performed three tests to ensure that this hypothesis holds in the selected cases. First, we determined the turbulence intensity $I = (v_{\text{rms}}/v_0)^2$ (v_0 being the mean bulk velocity and v_{rms} the root mean square of v fluctuations) to be in the range $[0.04\text{--}0.09]$ (i.e., $I \ll 1$); then, we found that the relation $f_{\rho_e}/f_{\rho_i} = \rho_i/\rho_e$ is fulfilled (for a detailed description of the test, see Sahraoui et al. 2012); and finally, we found good agreement between the probability density functions of spatial and temporal fluctuations of spacecraft C3 and C4 (for a detailed description of the test, see Vörös et al. 2006). Therefore, despite the low bulk velocity Taylor’s hypothesis holds in all the selected cases in this study.

We then process data using the method described in the previous section to study the spectral index and anisotropy of the obtained magnetic field PSDs (shown in the upper panels of Figures 2–5). To verify whether waves are present or not in the time intervals considered, and to clearly identify their nature (mirror, AIC, mixture of the two), we use the WHAMP program (Rönmark 1982). We also compute the thresholds for mirror and proton cyclotron instability in the $(T_{\perp}/T_{\parallel}, \beta_{i\parallel})$ parameter plane derived from the linear theory (see Hellinger et al. 2006; Bale et al. 2009). The thresholds are displayed in the lower panels of Figures 2–5. Since we aim to identify strong waves dominating the spectrum here, we choose the parameters corresponding to a strong growth rate $\gamma = 10^{-2}$ (Samsonov et al. 2001) to clearly differentiate between waves of different natures. Note that the observed results also hold (not shown) using a weaker growth rate $\gamma = 10^{-3}$ (Hellinger et al. 2006).

Figure 2 (upper panel) presents a case where no wave dominates the magnetic PSD. The spectrum is quasi-isotropic at all frequencies with a spectral index $\alpha \approx -2.8$ at $0.5 \text{ Hz} \leq f \leq 4 \text{ Hz}$. There is also a slight deviation from spectral isotropy at high frequencies, in the range $[5, 10]$ Hz, due to the presence of whistler waves. However, the study of the entire power spectrum of whistler waves in this case is not possible due to instrumental limitations, because the waveform data are limited to 12.5 Hz sampling. The absence of dominant wave activity is also demonstrated in the lower panel of Figure 2. The circles in color represents the magnetic field compressibility $C_{\parallel} = \delta B_{\parallel}^2 / (\delta B_{\parallel}^2 + \delta B_{\perp}^2)$ (Bale et al. 2009) plotted as a function

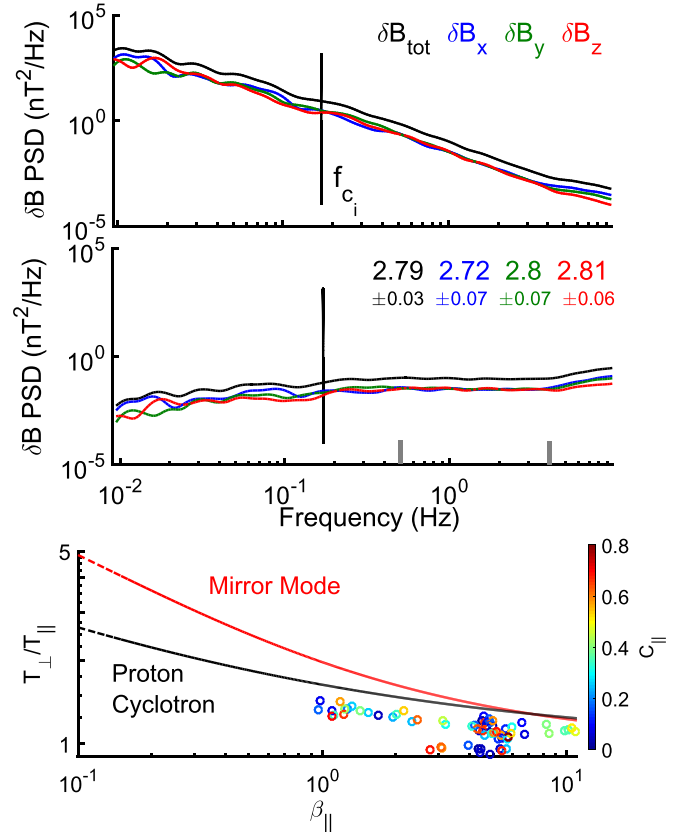


Figure 2. PSDs of δB measurements (upper panel) on board C3 on 2008 March 17 at 12:30–12:35. The solid lines indicate the observed magnetic field spectra (top panel) and the dashed lines indicate the compensated ($\delta B \times f^{|\alpha|}$) spectra (middle panel). The different components of δB are color-coded (top panel) along with the absolute value of their corresponding spectral index $|\alpha|$ (middle panel) and its uncertainty (calculated from the power-law fit with 95% confidence bounds), computed in the frequency range delimited by gray vertical lines. The gyrofrequency is indicated by the vertical black line. The thresholds for mirror (red) and proton cyclotron (black) instability are shown (as T_{\perp}/T_{\parallel} vs. $\beta_{i\parallel}$) in the bottom panel, for a relatively strong growth rate (for details see Samsonov et al. 2001): $\gamma = 10^{-2}$. Every 4 s of data is obtained, the color of which indicates the magnetic compressibility (see the color bar).

of T_{\perp}/T_{\parallel} and $\beta_{i\parallel}$. We see that every circle lies below the theoretically obtained thresholds for ion instability (red and black dotted curves), i.e., the fluctuations are stable against these ion instabilities.

Figure 3 shows the case where we observe the signature of mirror modes (δB_z dominates at $f < 0.05$ Hz) and no AIC waves (at $f \approx f_{ci}$). This is corroborated by the lower panel, in which almost every point lies on or is above the threshold for mirror instability. In this case the parallel component (δB_z) prevails in the high-frequency range and the fluctuations are non-gyrotropic, i.e., $\delta B_y > \delta B_x$ (Alexandrova et al. 2008b). While the indices δB_x and δB_y are close to -2.8 (except for the part > 6 Hz, due to whistlers), the parallel component δB_z is much less steep with $\alpha = -2$.

Figure 4 shows the case where AIC waves are observed. This can be seen because the perpendicular components B_x and B_y dominate the PSD at $0.04 \leq f \leq 0.2$, i.e., $\sim 0.1 - 0.5 f_{ci}$. With β_i mostly < 1 and the temperature anisotropy quite high (~ 2), most of the data points are concentrated around/above the threshold of the proton cyclotron instability (lower panels). The resulting spectra (upper panel) of B_x and B_y both have

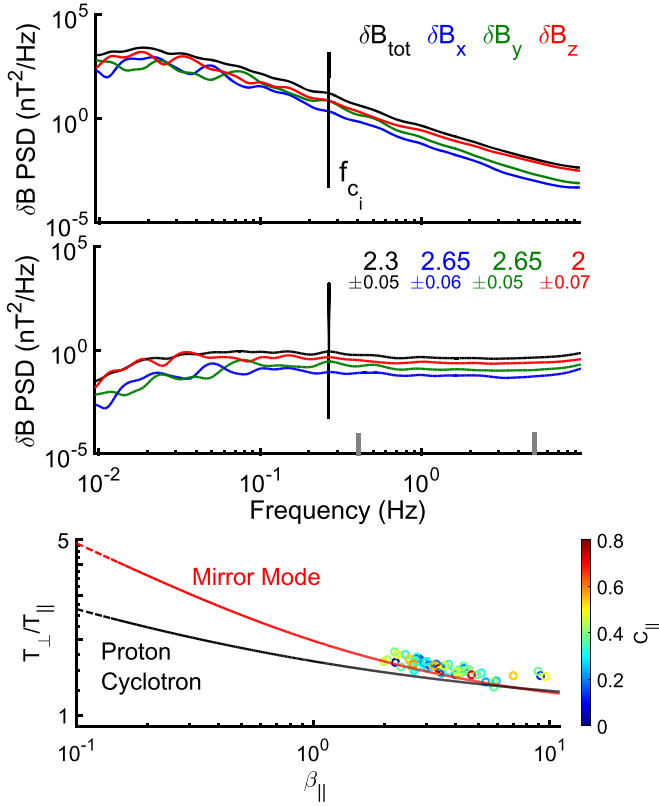


Figure 3. Same format as Figure 2, but for measurements on board C3 on 2008 March 25 at 07:01–07:05.

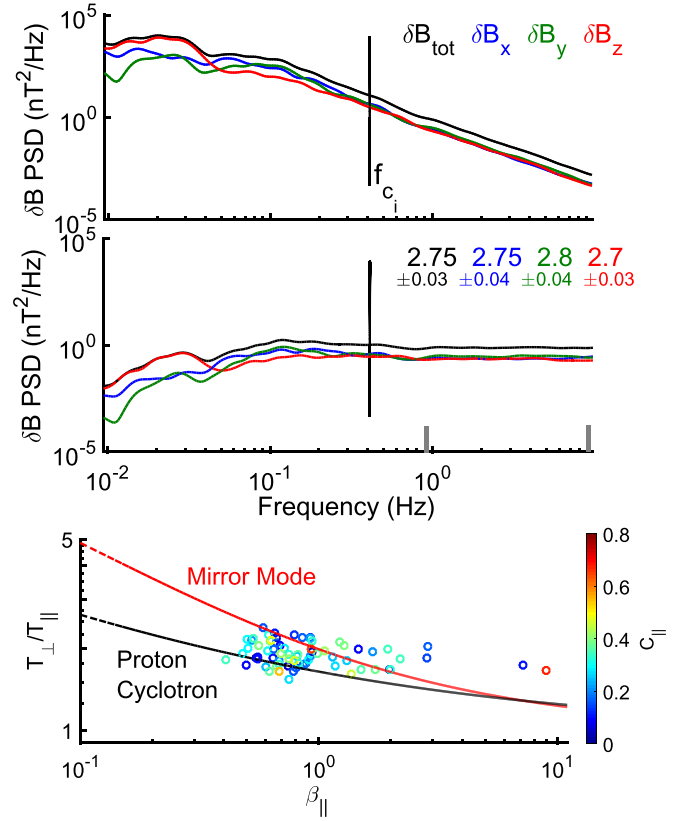


Figure 5. Same format as Figure 2, but for measurements on board C3 on 2008 March 25 at 06:51–06:56.

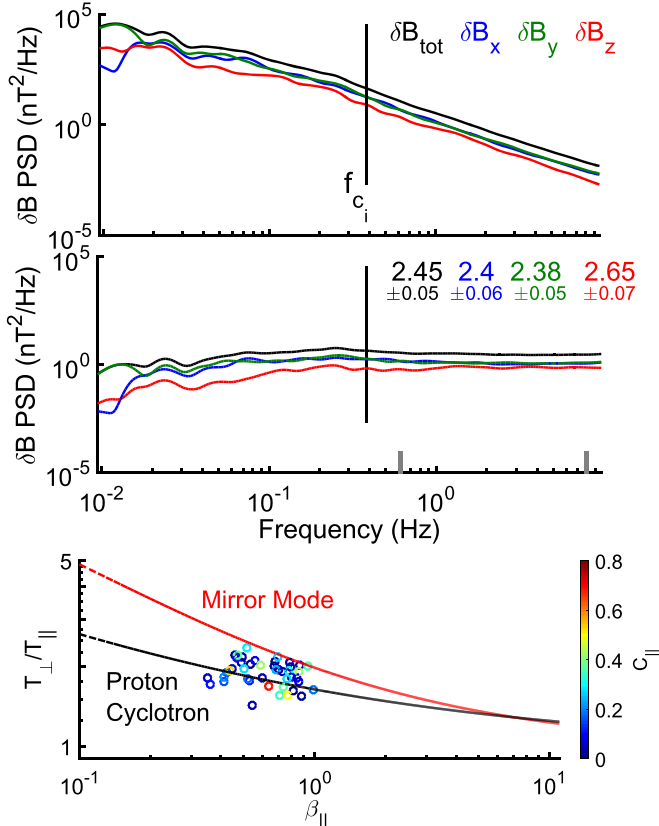


Figure 4. Same format as Figure 2, but for measurements on board C3 on 2008 March 30 at 01:35–01:39.

higher power than B_z in the high-frequency range and the fluctuations are gyrotropic, unlike in the previous case of mirror modes. The perpendicular components show a steepening at 0.25 Hz ($\sim 0.5f_{ci}$), whereas the parallel component displays a break at ~ 0.1 Hz. The fluctuations become slightly more isotropic close to the observed break, which can be due to a superposition of AIC waves and possible coherent structures with k_{\perp} at these frequencies, as has been observed in the solar wind by S. Lion et al. (2016, private communication). As a result, the total spectral index shows a steepening due to AIC waves at ~ 0.25 Hz. The spectral index for the parallel component is steeper ($\alpha = -2.65$) than for the perpendicular components ($\alpha \approx -2.4$).

Finally, Figure 5 presents a case where both mirror modes and AIC waves are observed; this is corroborated by the lower panel, where the plasma is unstable to both wave modes. Strong mirror modes dominate the spectrum at frequencies $f < 0.04$ Hz, whereas AIC waves prevail in the range $0.04 \text{ Hz} \leq f \leq 0.3$ Hz, where the spectral break is observed at $f \approx 0.1$ Hz ($\sim 0.4f_{ci}$). In the high-frequency range, the fluctuations are observed to be almost isotropic even though δB_y is slightly larger than δB_x and δB_z (see the following section for explanation). Interestingly, the total spectral index is close to -2.8 ($\alpha \approx -2.75$).

4. DISCUSSION AND SUMMARY

In this article, we study the effects of kinetic instabilities—in particular, mirror modes and AIC waves—on the small-scale turbulence in Earth’s magnetosheath in terms of magnetic field

anisotropy, spectral index, and spectral break at and above the ion scales using measurements from *Cluster* spacecraft.

First, we address the question of the scale responsible for the ion spectral break. We use cases of very high and low β_i to clearly separate spatial scales (ρ_i and λ_i). We provide three cases, each showing a different scale (ρ_i , λ_i , and f_{ci}) as the largest of the three. We show that, similarly to the solar wind (see Chen et al. 2014), a steepening occurs at the largest characteristic scale (i.e., at f_{\min_i}), which thus affects the spectrum first (Spangler & Gwinn 1990), regardless of its nature. However, we also demonstrate that at ion scales (i.e., in the range $f_{\min_i} \leq f \leq f_{\max_i}$), power spectra can be modified because of ion instabilities that are superposed on the background turbulence, and thus a power law is observed only at $f > f_{\max_i}$ (see Figure 1). Therefore, to study the small-scale cascade (down to electron scales) more accurately we suggest to define its onset at f_{\max_i} rather than at the break frequency.

Further we study the effects of mirror modes and AIC waves on the spectral index and anisotropy of magnetic field PSD in the high-frequency range ($f \in [0.2, 10]$ Hz, depending on cases). In the case where no strong waves dominate, we observe a “background” small-scale turbulence that is quasi-isotropic ($\delta B_x \approx \delta B_y \approx \delta B_z$). It has a spectral index $\alpha \approx -2.8$, which is consistent with scenarios of kinetic Alfvén waves (Howes 2008; Schekochihin et al. 2009), whistler modes (Stawicki et al. 2001; Gary & Smith 2009), and compressive Hall–MHD (Alexandrova et al. 2007, 2008a). When mirror modes prevail at ion scales ($f < f_{\rho_i}$), the parallel component is enhanced in the dispersive range (Czaykowska et al. 2001) and $\delta B_{\parallel} \gg \delta B_{\perp}$ can be observed (see Figure 3). Therefore, mirror modes can decrease the absolute value of the spectral index of amplitude fluctuations in the small-scale range, which is more likely to happen with large β_i (see also Alexandrova et al. 2008b). Further, along with mirror modes we observe non-gyrotropy (see also Figure 5), which can be explained by the fact that mirror modes have $\mathbf{k} \perp \mathbf{B}_0$, and therefore 2D turbulence is present, resulting in $\delta B_y > \delta B_x$ since δB_x has a component parallel to \mathbf{v} (see Bieber et al. 1996; Matthaeus et al. 2007, for details). Here $\delta B_y = 2\delta B_x$, which is consistent with the model of 2D turbulence developed in the cited papers. In cases where \mathbf{v} is not low, this non-gyrotropy can also be reinforced by Doppler-shift effects as stated above (see also Alexandrova et al. 2008b).

In contrast, when AIC waves prevail at ion scales, perpendicular components dominate in the high-frequency range and the fluctuations are observed to be gyrotropic (see Figure 4), because AIC waves have $\mathbf{k} \parallel \mathbf{B}_0$ and thus slab turbulence is present, resulting in $\delta B_x = \delta B_y$ due to the axisymmetric condition (see again Bieber et al. 1996; Matthaeus et al. 2007, for details). In the presence of either strong mirror or AIC waves at ion scales, the absolute value of the spectral index of the parallel or perpendicular components, respectively, is decreased ($|\alpha| \approx 2-2.7$). However, when both types of waves are observed simultaneously (see Figure 5), \mathbf{k} -vectors are mixed and thus a composite of 2D and slab turbulence is present (Bieber et al. 1996). This results in a smaller non-gyrotropy (here $\delta B_y = 1.2\delta B_x$) and the fluctuations become more isotropic (Alexandrova et al. 2008b). In Figure 5, the resulting spectral index is decreased ($|\alpha| \approx 2.75$) but close to -2.8 . This could be due to the fact that in this case the instabilities are already developed, and thus the energy of waves is lost to particles by wave–particle interaction at ion

scales and does not cascade toward higher frequencies. Therefore we mostly observe the background turbulence, whereas the cases in Figures 3 and 4 could correspond to the developing phase of the ion instabilities. However, this question requires a detailed study and is left for future investigation.

In summary, in this article the clear identification of kinetic instabilities in magnetic spectra provides experimental evidence showing that in Earth’s magnetosheath: (1) the break of power spectra of magnetic field fluctuations occurs at the largest characteristic ion scale, regardless of its nature; (2) ion instabilities that are superposed on the background turbulence can, depending on the plasma parameters, modify the spectra up to f_{\max_i} (corresponding to the smallest ion scale), and thus we suggest to define the onset of the small-scale cascade at f_{\max_i} rather than at the break frequency; (3) in the small-scale range, when no waves are observed, the background turbulence is quasi-isotropic ($\delta B_x \approx \delta B_y \approx \delta B_z$) with an index of -2.8 , consistent with kinetic Alfvén waves, whistler, and compressive Hall–MHD scenarios; (4) the observed non-gyrotropy of kinetic amplitude fluctuations can be due to a 2D turbulence developing in the presence of mirror modes (i.e., $\mathbf{k} \perp \mathbf{B}_0$), whereas gyrotropic amplitude fluctuations result from the possible development of slab turbulence in the presence of AIC waves (i.e., $\mathbf{k} \parallel \mathbf{B}_0$); (5) when strong waves dominate, the absolute values of spectral indices of the corresponding components are decreased ($|\alpha| < 2.8$); (6) the presence of both waves reduces the anisotropy of amplitude fluctuations in the small-scale range, probably because of a combination of 2D and slab turbulence.

In conclusion, we point out that the power spectra at ion scales in Earth’s magnetosheath are highly dependent on local plasma parameters and ion instabilities. Thus, in order to interpret them correctly, it is necessary to identify the local inhomogeneities (waves, structures) and take into account their respective effects on the turbulence at ion scales and in the small-scale range.

H.B.’s and E.Y.’s research has received funding from the European Community’s Seventh Framework Programme ([7/2007–2013]) under grant agreement n°313038/STORM. Wavelet software was provided by C. Torrence and G. Compo, and is available at <http://atoc.colorado.edu/research/wavelets/>.

REFERENCES

- Alexandrova, O., Carbone, V., Veltri, P., & Sorriso-Valvo, L. 2007, *P&SS*, **55**, 2224
- Alexandrova, O., Carbone, V., Veltri, P., & Sorriso-Valvo, L. 2008a, *ApJ*, **674**, 1153
- Alexandrova, O., Chen, C. H. K., Sorriso-Valvo, L., Horbury, T. S., & Bale, S. D. 2013, *SSRv*, **178**, 101
- Alexandrova, O., Lacombe, C., & Mangeney, A. 2008b, *AnGeo*, **26**, 3585
- Alexandrova, O., Mangeney, A., Maksimovic, M., et al. 2006, *JGRA*, **111**, 12208
- Bale, S. D., Kasper, J. C., Howes, G. G., et al. 2009, *PhRvL*, **103**, 211101
- Balogh, A., Carr, C. M., Acuña, M. H., et al. 2001, *AnGeo*, **19**, 1207
- Bieber, J. W., Wanner, W., & Matthaeus, W. H. 1996, *JGR*, **101**, 2511
- Bruno, R., & Carbone, V. 2013, *LRSP*, **10**, 2
- Chen, C. H. K., Leung, L., Boldyrev, S., Maruca, B. A., & Bale, S. D. 2014, *GeoRL*, **41**, 8081
- Cornilleau-Wehrin, N., Chauveau, P., Louis, S., et al. 1997, *SSRv*, **79**, 107
- Czaykowska, A., Bauer, T. M., Treumann, R. A., & Baumjohann, W. 2001, *AnGeo*, **19**, 275
- Dmitruk, P., Matthaeus, W. H., & Seenu, N. 2004, *ApJ*, **617**, 667
- Galtier, S. 2006, *JPIPh*, **72**, 721

- Gary, S. P., & Smith, C. W. 2009, *JGRA*, **114**, 12105
- Hellinger, P., Trávníček, P., Kasper, J. C., & Lazarus, A. J. 2006, *GeoRL*, **33**, 9101
- Howes, G. G. 2008, *PhPI*, **15**, 055904
- Klein, K. G., Howes, G. G., & TenBarge, J. M. 2014, *ApJL*, **790**, L20
- Leamon, R. J., Matthaeus, W. H., Smith, C. W., et al. 2000, *ApJ*, **537**, 1054
- Lion, S., Alexandrova, O., & Zaslavsky, A. 2016, *ApJ*, **824**, 47
- Matteini, L., Hellinger, P., Goldstein, B. E., et al. 2013, *JGRA*, **118**, 2771
- Matteini, L., Landi, S., Hellinger, P., et al. 2007, *GeoRL*, **34**, 20105
- Matthaeus, W. H., Bieber, J. W., Ruffolo, D., Chuychai, P., & Minnie, J. 2007, *ApJ*, **667**, 956
- Rème, H., Aoustin, C., Bosqued, J. M., et al. 2001, *AnGeo*, **19**, 1303
- Rönmark, K. 1982, Computation of the Dielectric Tensor of a Maxwellian Plasma, Tech. Rep.
- Russell, C. T. 1972, *NASSP*, **308**, 365
- Sahraoui, F., Belmont, G., & Goldstein, M. L. 2012, *ApJ*, **748**, 100
- Sahraoui, F., Belmont, G., Rezeau, L., et al. 2006, *PhRvL*, **96**, 075002
- Samsonov, A. A., Pudovkin, M. I., Gary, S. P., & Hubert, D. 2001, *JGR*, **106**, 21689
- Schekochihin, A. A., Cowley, S. C., Dorland, W., et al. 2009, *ApJS*, **182**, 310
- Schwartz, S. J., Burgess, D., & Moses, J. J. 1996, *AnGeo*, **14**, 1134
- Shevyrev, N. N., Zastenker, G. N., Eiges, P. E., & Richardson, J. D. 2006, *AdSpR*, **37**, 1516
- Spangler, S. R., & Gwinn, C. R. 1990, *ApJL*, **353**, L29
- Stawicki, O., Gary, S. P., & Li, H. 2001, *JGR*, **106**, 8273
- Torrence, C., & Compo, G. P. 1998, *BAMS*, **79**, 61
- Vörös, Z., Baumjohann, W., Nakamura, R., Volwerk, M., & Runov, A. 2006, *SSRv*, **122**, 301
- Zimbaro, G., Greco, A., Sorriso-Valvo, L., et al. 2010, *SSRv*, **156**, 89